

Observation of Two-Photon Above-Threshold Ionization of Rare Gases by xuv Harmonic Photons

Naoki Miyamoto,¹ Masato Kamei,¹ Dai Yoshitomi,¹ Teruto Kanai,¹ Taro Sekikawa,¹
Takashi Nakajima,^{1,2} and Shuntaro Watanabe¹

¹*Institute for Solid State Physics, University of Tokyo, 5-1-5 Kashiwanoha, Kashiwa 277-8581, Japan*

²*Institute of Advanced Energy, Kyoto University, Gokasho, Uji, Kyoto 611-0011, Japan*

(Received 18 February 2004; published 19 August 2004)

We have successfully observed two-photon above-threshold ionization in rare gas atoms (Ar, Xe, and He) by the fifth harmonic (25 eV photon energy) of a KrF laser. Use of the energy-resolved photoelectron counting system together with our laser, providing strong 25 eV radiation at 40–100 Hz, enabled us to detect the very weak single-color two-photon above-threshold ionization signals. Experimental data are in good agreement with our theoretical calculations newly developed along the line of multichannel quantum defect theory.

DOI: 10.1103/PhysRevLett.93.083903

PACS numbers: 42.65.Ky, 32.80.Rm

Recent progress in the research of high harmonics has broken the record of pulse duration into the attosecond time scale and opened the doorway to attosecond metrology [1–4]. The use of ultrashort harmonic pulses has enabled us to observe the relaxation of inner shell hole and Auger decay in the time domain [5–7].

In the visible wavelength, ultrashort pulses are characterized by methods such as frequency-resolved optical gating (FROG) [8] and spectral phase interferometry for direct electric-field reconstruction (SPIDER) [9], where the shape and the phase of the pulse can be determined at the same time. However, the temporal width of the attosecond pulses was only indirectly estimated so far with the aid of a theoretical simulation, which requires the deep knowledge on the harmonic generation mechanism. Obviously, the direct and full characterization of harmonic pulses approaching the attosecond time domain in the short wavelength is definitely required not only to study the further details of harmonic generation mechanism but also to apply harmonics to investigate various ultrafast dynamics.

Until now the pulse width of the harmonics has been measured by the autocorrelation-based method [4,10,11]. The phase was also measured by two-photon ionization FROG [12]. Limitation of these methods is that they were applicable only in the relatively long wavelength where the photon energies were still below the ionization threshold of rare gases. In the shorter wavelength, due to the insufficient intensity and detection sensitivity to observe nonlinear processes by single color, the cross-correlation-based method was used to determine the pulse width of harmonics [13–15]. The phase was recently measured by the cross-correlation-based FROG (XFROG) [16]. In other words, the two-color (9ω and ω photons) above-threshold ionization (ATI) signal was used for XFROG. Note that the lower limit of the measurable pulse width is imposed by the pulse width of reference pulses for the

usual cross correlation, while it is limited by the optical period of 2.7 fs at 800 nm for FROG or SPIDER.

In order to lift these restrictions on the measurable pulse durations, observation of single-color two-photon ATI is an important cornerstone toward the “full and direct” characterization of ultrashort pulses in the extreme ultraviolet (xuv)-soft x-ray range, which may have an attosecond pulse duration [17]. This is because (i) for xuv photons even a single-photon absorption will bring atoms above ionization threshold and hence ATI is necessarily involved for any nonlinear processes, and (ii) the accuracy of autocorrelation-based pulse measurement has no fundamental limitation in terms of the measurable pulse width. In the shorter wavelength (xuv-soft x-ray), however, we should keep in mind that bright light sources are not easily obtained and the corresponding dipole moments are much smaller than those in the visible-IR range [18], since large transition energy usually means small overlap of wave functions. It should be clear by now that the observation of single-color ATI by harmonic photons is far more difficult than two-color ATI. About the theoretical aspects for the description of two-photon ATI, we are not aware of any calculations which resolve fine structure of the ionic core.

In this Letter, we report the first experimental observation of single-color two-photon ATI in Ar, Xe, and He in the xuv range at 25 eV photon energy and compare with our theoretical results. Since the single-color two-photon ATI signal by xuv photons is very weak, a special detection technique is needed. This was realized by the use of the energy-resolved electron counting system at a low repetition rate of 40–100 Hz together with strong 25 eV radiation generated by the fifth harmonic of our KrF/Ti:sapphire hybrid laser system.

The KrF/Ti:sapphire hybrid laser system has been used to generate 25 eV radiation. Each shot contains four (two *s*-polarized and two *p*-polarized) pulses separated by

2.5 ns [19]. Figure 1 shows the experimental setup. Only p -polarized pulses were selected and focused with an $f = 1$ m mirror into a neon gas jet. The pulse energies of the fifth harmonic at the location of the source are $1.2 \mu\text{J}$ at 10 Hz and $0.14 \mu\text{J}$ at 200 Hz, respectively, depending on how the gas jet is driven: At the first stage of our experiment for Ar and Xe, a magnetically driven gas jet was used at 40 Hz, while a piezoelectrically driven gas jet was used at 100 Hz for He to increase the photoelectron yield. The fundamental energy was reduced to 1% with the beam splitter designed for p polarization. The residual fundamental and third harmonic pulses were eliminated almost completely with the $0.15 \mu\text{m}$ -thick Al filter. The fifth harmonic was selected with an $f = 20$ cm concave Sc/Si multilayer mirror. The higher (≥ 7 th) harmonics were reduced to the negligible level by the Sc/Si multilayer mirror designed for 49.6 nm. The fifth harmonic reflected by the $f = 20$ cm multilayer mirror was focused into a diameter of $2 \mu\text{m}$ [20]. The rare gases used for ionization were continuously supplied from a metal tube with a 0.7 mm inside diameter. The gas pressure for ionization was 1 Torr in the interaction region. The background pressure of the ionization chamber was kept at $\sim 5 \times 10^{-5}$ Torr by the differential pumping against the harmonic chamber. Optical alignment of the harmonic pulse was taken by using the fundamental pulses without the Al filter. On-target pulse energy of the fifth harmonic was measured with an xuv photodiode, and the temporal width of the fifth harmonic pulse was estimated to be 210 fs from the $1/\sqrt{5}$ law with respect to the fundamental pulse width. Photoelectrons were detected with a 100-mm semispherical photoelectron spectrometer, placed along the line of the polarization direction, with an electron counting system. The quantum efficiency of the detector (channeltron) is about 15%. The full acceptable angle of the electrostatic lens attached to the analyzer is 24° around the polarization direction.

Figure 2 shows the level diagrams of Ar, Xe, and He, respectively. The photon energy of 25 eV is already above the first ionization thresholds of all rare gases. Note that the two-photon absorption of 25 eV photons bring Ar and Xe atoms above the double ionization thresholds. Thus, two-photon double ionization as well as two-photon ATI can take place for Ar and Xe. However, as reported in Ref. [18], the two-photon double ionization cross section

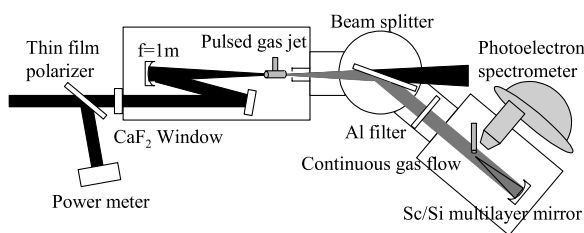


FIG. 1. Experimental setup for the two-photon ATI measurement.

is typically about 1 order of magnitude smaller than that for the two-photon ATI cross section. Besides, the photoelectron spectrum for the two-photon double ionization appears as a background, showing no peak structure. Therefore, as we report in this Letter, it is a natural choice, in particular, as a first attempt in the xuv range, to try to observe two-photon ATI. The peaks due to two-photon ATI should be located at 34.24 and 34.06 eV in Ar, 37.87 and 36.56 eV in Xe, and 25.41 eV in He, respectively.

Figure 3(a) shows the two-photon ATI spectrum of Ar. The right vertical axis shows counted electrons/900 s, while the left axis corresponds to electrons/pulse by considering two pulses included in a single shot at 40 Hz. The harmonic energy was 1.2 nJ and the focused intensity was 120 GW/cm^2 . The two peaks separated by 0.18 eV were resolved. The branching ratio, defined as the ratio of photoelectron yield leaving the $p^5[{}^2P_{1/2}]$ core to that of the $p^5[{}^2P_{3/2}]$ core, was about 0.75 and the total detected photoelectrons within two peaks (the hatched area) were 70/900 s, corresponding to 9.7×10^{-4} /pulse. Next, the two-photon ATI spectrum of Xe is shown in Fig. 3(b). The harmonic energy was 1.5 nJ at 40 Hz, giving the focused intensity of 150 GW/cm^2 . In Fig. 3(b), only a single peak corresponding to the core of $p^5[{}^2P_{3/2}]$ was observed. The background noise may have covered the two-photon ATI signal for the $p^5[{}^2P_{1/2}]$ core. The total detected photoelectrons within the peak (the hatched area) were 38/420 s, corresponding to 1.1×10^{-3} /pulse. Finally, the two-photon ATI spectrum of He is shown in Fig. 3(c). The harmonic pulse energy was 1.2 nJ at 100 Hz. The focused intensity was estimated to be 120 GW/cm^2 . The total number of photoelectrons was 48/360 s, corresponding to 4.2×10^{-4} counts/pulse. The spectral width (FWHM) of the fifth harmonic is estimated to be 170 meV from the spectra of single-photon ionization. For the spectra of two-photon ATI, the counting system was set to the rather large energy increment (25 meV in He and 100 meV in Ar and Xe, respectively)

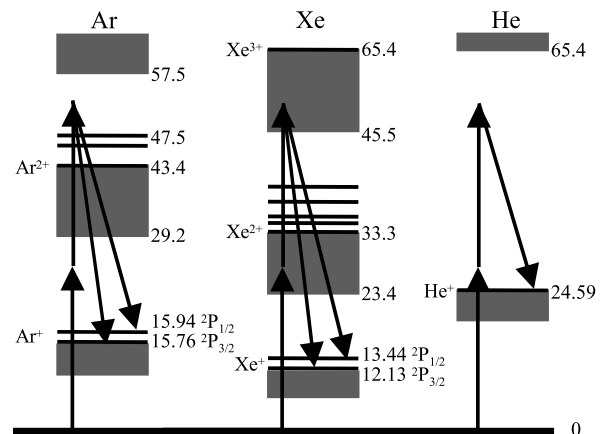


FIG. 2. The level diagrams of Ar, Xe, and He relevant to the two-photon ATI by 25 eV photons.

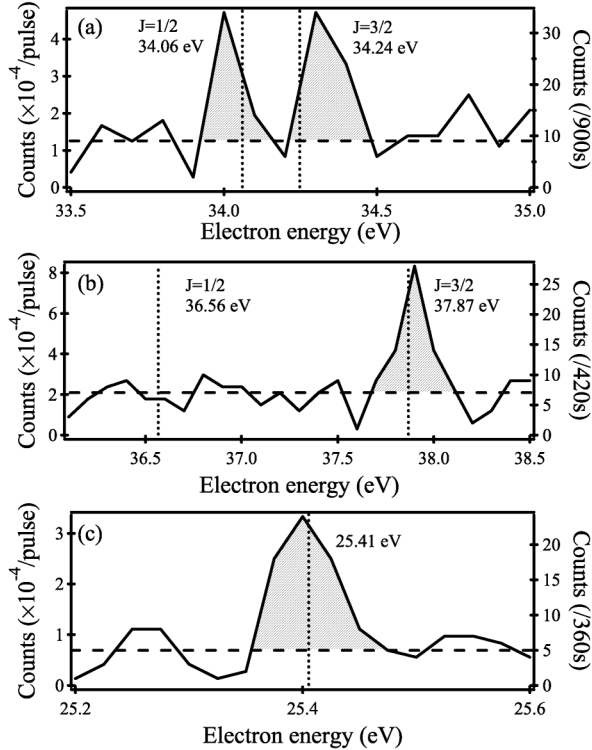


FIG. 3. Photoelectron spectra of two-photon ATI in (a) Ar, (b) Xe, and (c) He.

and to the corresponding resolution (40 meV in He and 100 meV in Ar and Xe, respectively). This is a compromise of the weak two-photon ATI signal and the fast energy scan and data accumulation needed for the measurement. Therefore, the measured spectral shape of two-photon ATI may not reflect the real spectral shape.

The experimental results can be compared with the theoretical calculation. For He, the two-photon ATI cross section can be found in the literature [18]. The total number Y of the generated photoelectrons by two-photon ATI were given by [21]

$$Y = \sigma^{(2)} n \int dt \int d^3\mathbf{r} F^2(\mathbf{r}, t), \quad (1)$$

where n is the gas density ($3.6 \times 10^{16}/\text{cm}^3$) and $F(\mathbf{r}, t)$ is the photon flux in photons $\text{cm}^{-2} \text{s}^{-1}$. We assumed the temporal Gaussian profile and the focusing of the Gaussian beam with $M^2 = 12$ [20].

The angular distribution of photoelectrons is expressed for 25 eV photons by [22]

$$\frac{d\sigma^{(2)}}{d\Omega} = a(0.729\cos^4\theta - 0.345\cos^2\theta + 0.075), \quad (2)$$

where a is a constant and θ is the angle from the polarization direction. The electron counted by the analyzer is 0.7% of the total ejected electrons from the acceptable angle of the electrostatic lens (4.5%) and the quantum efficiency of the channeltron (15%). By using the laser intensity of 120 GW/cm^2 , and the two-photon ATI cross

section of $1 \times 10^{-52} \text{ cm}^4 \text{ s}$ [18], the anticipated electron count is estimated to be $3.6 \times 10^{-4}/\text{pulse}$. This value is in good agreement with the experiment ($6.7 \times 10^{-4}/\text{pulse}$).

For Ar and Xe, however, we have to carry out theoretical calculations since no theoretical data are available in the literature for the two-photon ATI processes by xuv photons. For rare gas atoms other than He, all excited bound states have configurations of p^5nl , where n and l are the principal quantum number and orbital angular momentum of the excited electron, respectively, and continuum states have configurations such as $p^5\epsilon l$ and $p^4nl\epsilon l'$, etc., with ϵ being the photoelectron energy. It is far from trivial to take into account all interactions between electrons in open subshells. Note that most of the time-dependent calculations for rare gas atoms reported so far do not include spin-orbit interactions [23,24], which could be sufficient in the tunneling regime for small photons. At the present study, however, it is essential that the theory explicitly incorporates spin-orbit interactions since experimental photoelectron spectra resolve $p^5[{}^2P_{3/2}]$ and $p^5[{}^2P_{1/2}]$ core states. Because of this fact, we have developed a theoretical method, using multichannel quantum defect theory (MQDT) wave functions, with a combined use of the length and acceleration gauge so that the free-free transition can be calculated without divergence [25]. Briefly, the total MQDT wave function can be written as a linear combination of the hydrogenlike wave functions. Needless to say, the advantage of the use of MQDT is that it effectively incorporates not only spin-orbit interactions but also the configuration mixing to some extent. On the other hand, the limitation of the present approach is that we can include only two lowest core states, $p^5[{}^2P_{3/2}]$ and $p^5[{}^2P_{1/2}]$.

In order to calculate two-photon ATI cross sections and the branching ratios perturbatively, we need the following quantities: (i) ground($J=0$)-bound($J=1$) and (ii) ground($J=0$)-free($J=1$) dipole moments for the first transition and (iii) bound($J=1$)-free($J=0$ or 2) and (iv) free($J=1$)-free($J=0$ or 2) dipole moments for the second transition. For (i), empirical MQDT dipole moments fitted to the experimental spectra have been used. As for the ground-free dipole moments experimental single-photon ionization cross sections are available [26]. While keeping the ratios of dipole moments for all channels used for (i), scaling has been made as a function of photon energy to fit the cross section data. This way ground-free dipole moments have been determined for (i). Now for (iii), bound state and continuum wave functions are generated using the MQDT parameters. Note that we have included a linear energy dependence of the MQDT parameters for the bound states, while an energy dependence for the continuum states has been fixed to the values at the $p^5[{}^2P_{1/2}]$ threshold. For (iv), it is well known that the dipole moment does not converge if the length gauge is used.

TABLE I. Comparison between the experimental and theoretical results of photoelectron yields and branching ratios in He, Ar, and Xe.

| | | Experiment | Theory |
|----|-----------------|----------------------|----------------------|
| He | Yield(/pulse) | 6.7×10^{-4} | 3.6×10^{-4} |
| Ar | Yield(/pulse) | 9.7×10^{-4} | 8.0×10^{-4} |
| | branching ratio | 0.75 | 0.30 |
| Xe | Yield(/pulse) | 1.1×10^{-3} | 5.4×10^{-3} |
| | branching ratio | ≤ 0.2 | 0.44 |

One way to circumvent this convergence problem is to employ the combination of the length gauge for small radius, $0 < r < R$ [typically $R = 20\text{--}30$ (a.u.)], and the acceleration gauge for $R < r < \infty$ together with the surface terms [27]: Having checked that the free-free dipole moments calculated this way for hydrogen agree very well ($<1\%$ difference) with those by the Green function method, we performed calculations for Ar and Xe. Now the ground-bound-free contribution to the transition amplitude of two-photon ATI from the ground state $|g\rangle$ to the final continuum of channel k_2 described by $|f, k_2\rangle$ via intermediate bound states $|m\rangle$ can be calculated using the formula

$$M_{\text{gbf}}^{(2)} = \sum_{k_2} \sum_m \frac{\langle f, k_2 | D | m \rangle \langle m | D | g \rangle}{E_g + \omega - E_m}, \quad (3)$$

where D is the dipole operator in the length gauge and ω is a photon energy. Note that all matrix elements are in the length gauge. Similarly, the ground-free-free contribution is calculated as

$$M_{\text{gff}}^{(2)} = \frac{1}{\omega^4} \left[P \sum_{k_2} \sum_{m, k_1} \frac{\langle f, k_2 | A | m, k_1 \rangle \langle m, k_1 | A | g \rangle}{E_g + \omega - E_m} - i\pi \langle f, k_2 | A | m_0, k_1 \rangle \langle m_0, k_1 | A | g \rangle \right], \quad (4)$$

where A is the dipole operator in the acceleration gauge. P indicates that the principal value integral must be taken at the pole m_0 of channel k_1 with energy $E_{m_0} = E_g + \omega$. After all these procedures, the two-photon ATI cross sections for 25 eV photons have been calculated to be $2.0 \times 10^{-51} \text{ cm}^4 \text{ s}$ and $1.0 \times 10^{-51} \text{ cm}^4 \text{ s}$ for Ar and Xe, respectively [25]. By taking into account the angular distribution of photoelectrons into the detector, the branching ratios integrated over all solid angles and that within the acceptable angle are calculated to be 0.38 and 0.30 for Ar and 0.42 and 0.44 for Xe for 25 eV photons, respectively. The collection efficiency within the acceptable angle is 0.5% in Ar and 4.3% in Xe. Our theory is compared with our experiment in Table I.

In summary, we have reported the first experimental observation of two-photon ATI in rare gas atoms by the fifth harmonic (photon energy 25 eV) of the KrF laser and compared with our corresponding theoretical results.

Considering the experimental ambiguity of the xuv intensity and the various approximations used for theoretical calculations, our experimental and theoretical results agree rather well in terms of the two-photon ATI signals. However, the branching ratios did not show very good agreement. Before closing this Letter, we briefly mention that we have recently succeeded in observing single-color two-photon ATI of He using the ninth harmonic (27.9 eV) of a frequency-doubled Ti:sapphire laser with a kilohertz repetition rate. Autocorrelation measurement is now under progress at this photon energy.

- [1] Ivan P. Christov, Margaret M. Murnane, and Henry C. Kapteyn, *Phys. Rev. Lett.* **78**, 1251 (1997).
- [2] M. Hetschel *et al.*, *Nature (London)* **414**, 509 (2001).
- [3] P. M. Paul *et al.*, *Science* **292**, 1689 (2001).
- [4] P. Tzallas, D. Charalambidis, N. A. Papadogiannis, K. Witte, and G. D. Tsakiris, *Nature (London)* **426**, 267 (2002).
- [5] M. Drescher *et al.*, *Nature (London)* **419**, 803 (2002).
- [6] T. Sekikawa, T. Yamazaki, Y. Nabekawa, and S. Watanabe, *J. Opt. Soc. Am. B* **19**, 1941 (2002).
- [7] T. Shimizu, T. Sekikawa, T. Kanai, S. Watanabe, and M. Itoh, *Phys. Rev. Lett.* **91**, 017401 (2003).
- [8] R. Trebino *et al.*, *Rev. Sci. Instrum.* **68**, 3277 (1997).
- [9] C. Iacosis and I. A. Walmsley, *IEEE J. Quantum Electron.* **35**, 501 (1999).
- [10] Y. Kobayashi, T. Sekikawa, Y. Nabekawa, and S. Watanabe, *Opt. Lett.* **23**, 64 (1998).
- [11] T. Sekikawa, T. Ohno, T. Yamazaki, Y. Nabekawa, and S. Watanabe, *Phys. Rev. Lett.* **83**, 2564 (1999).
- [12] T. Sekikawa, T. Katsura, S. Miura, and S. Watanabe, *Phys. Rev. Lett.* **88**, 193902 (2002).
- [13] T. E. Glover, R. W. Schoenlein, A. H. Chin, and C. V. Shank, *Phys. Rev. Lett.* **76**, 2468 (1996).
- [14] J. M. Schins *et al.*, *J. Opt. Soc. Am. B* **13**, 197 (1996).
- [15] J. Norin *et al.*, *Phys. Rev. Lett.* **88**, 193901 (2002).
- [16] T. Sekikawa, T. Kanai, and S. Watanabe, *Phys. Rev. Lett.* **91**, 103902 (2003).
- [17] T. Nakajima and L. A. A. Nikolopoulos, *Phys. Rev. A* **66**, 041402(R) (2002).
- [18] L. A. A. Nikolopoulos and P. Lambropoulos, *J. Phys. B* **34**, 545 (2001).
- [19] Y. Nabekawa, D. Yoshitomi, T. Sekikawa, and S. Watanabe, *Opt. Lett.* **26**, 807 (2001).
- [20] D. Yoshitomi, T. Shimizu, T. Sekikawa, and S. Watanabe, *Opt. Lett.* **27**, 2170 (2002).
- [21] A. Saenz and P. Lambropoulos, *J. Phys. B* **32**, 5629 (1999).
- [22] Takashi Nakajima (unpublished).
- [23] K. C. Kulander and T. N. Rescigno, *Comput. Phys. Commun.* **63**, 523 (1991).
- [24] H. G. Muller, *Phys. Rev. A* **60**, 1341 (1999).
- [25] Takashi Nakajima and Shuntaro Watanabe (unpublished).
- [26] J. A. R. Samson and R. B. Cairns, *Phys. Rev.* **173**, 80 (1968).
- [27] M. J. Seaton, *J. Phys. B* **19**, 2601 (1986).